Journal of Engineering and Architecture
December 2020, Vol. 8, No. 2, pp. 42-49
ISSN: 2334-2986 (Print), 2334-2994 (Online)

Published by American Research Institute for Policy Development
DOI: 10.15640/jea.v8n2a7
URL: https://doi.org/10.15640/jea.v8n2a7

Design and Characterization of a Translucent Solar Module (TSM) for Greenhouse Structures

Remington S. Ketchum[1], Hao-Chih Yuan[2], Liliana Ruiz-Diaz,[1] Nicholas P. Lyons,[1] Sifang Cui,[1] Michael Frasier,[2] Sasaan A. Showghi,[1] Kyung-Jo Kim,[1] Aletheia Ida[3], Wei Pan,[2] and Robert A. Norwood[1]

Abstract

There exist numerous advantages of using building integrated photovoltaic (BIPV) technology, including efficient use of solar energy, control of indoor illumination, and reduced energy use for cooling and heating. Current pioneer BIPV technologies have not been fully deployed due to lack of standardization, low adaptability, and moderate efficiency. Here we present a novel, effective, and reliable translucent solar module (TSM) which uses sparsely populated bifacial silicon (Si) photovoltaic (PV) cells and concentrating spectrum-selective dichroic reflectors to illuminate greenhouses and buildings while capturing near infrared light to enhance output. The TSM can be optimized for different applications by changing the dichroic design, varying the shape of the reflector, and altering the tilt-angle of the framing integration with greenhouse structures. Experimental results from a 410 x 500 mm² proof-of-concept TSM show excellent agreement with theoretical values, demonstrating a field-of-view (*FOV*) collection of ±23° and generating up to ~30% more power than a traditional Si PV panel.

Keywords: photovoltaics, translucent solar module, greenhouse structures, dichroic reflectors, bifacial silicon

1. Introduction

Photovoltaics (PVs) are becoming more reliable and cost-effective. Installing PV systems to convert sunlight into electricity is not just desirable because of environmental reasons, but as a result of economic drivers (Parida, Iniyan & Goic, 2011; Philipps, 2019). One sector that has great potential is building integrated PV (BIPV), where solar panels are incorporated as integral parts of buildings or greenhouses, displacing building material cost, and generating electricity without adding real estate. However, barriers like lack of standards and the complex dynamic between planners, developers, architects, engineers, and installers have restricted the current expansion of BIPV(Heinstein, Ballif & Perret-Aebi, 2013;Hassanien, Li & Lin, 2016).Additionally, in the case of transmissive BIPV, one has to consider how much sunlight can be portioned for renewable energy generation before the reduced irradiance drastically impacts the visual comfort of building tenants or the yield of the farm produce.

The optical spectra that are optimum for human vision and plant growth share some similarities. The rod and cone photoreceptors in the human eye are sensitive only to the spectrum between~400 to 700 nm wavelengths (Brown & Wald, 1964). Plants require exposure to specific spectra of light for effective photosynthesis. The absorption of the photoreceptors in plants varies from species to species, but they mainly absorb blue and red light, as depicted in Fig. 1a (Bisegna, Burattini & Mattoni, 2015). Green light, even though not heavily absorbed, still plays a role by driving photosynthetic activity deeper within the leaves(Sun, Nishio & Vogelmann, 1998) and thus, the International Commission on Illumination (CIE) defines the 400 to 700 nm spectrum as photosynthetically active radiation(PAR) (Tibbits, 1993). The spectrum >700 nm, i.e. infrared (IR) range, does not contribute to photosynthesis nor can it be seen by the human eye. Moreover, excessive transmitted IR from the sun heats up the interior space of buildings and, as a result, can drive up demand for cooling and water irrigation. In the U.S., commercial buildings, heating and cooling account for ~35% of the energy consumption (US EIA, 2016) and as much as ~80% in soilless hydroponic greenhouse farming (Barbosa, Gadelha, Kubik, Proctor, Reichelm, Weissinger, Wohlleb & Halden, 2015).

[1] James C. Wyant College of Optical Sciences, University of Arizona, 1630 E. University Blvd., Tucson, AZ, 85721, USA
[2] DWP Energy Solutions, LLC, 18110 SE 34th Street Building 4, Suite 480, Vancouver, WA, 98683
[3] College of Architecture, Planning and Landscape Architecture, University of Arizona, 1040 N. Olive Rd., Tucson, AZ, 85721, USA

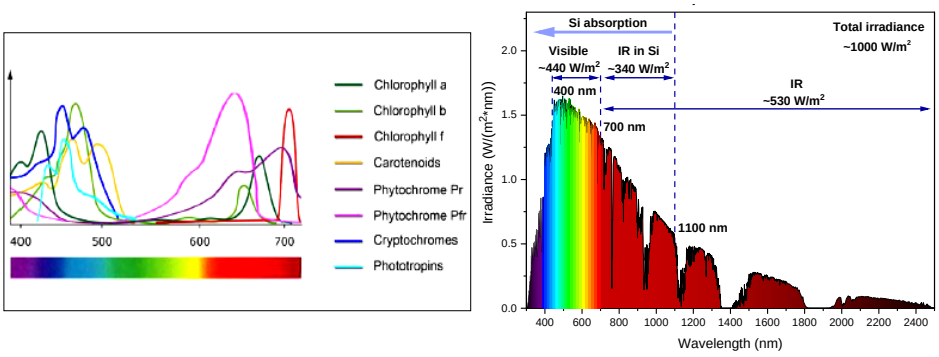

Figure1. Absorption spectra of plants and the solar spectrum: a) plants photoreceptors absorb mostly blue and red light. Image adapted from [6]; b) spectral irradiance of AM1.5 spectrum and absorption of a typical Si solar cell. Values taken from [15].

In greenhouse applications of BIPV, ideally one would like to have a PV panel that preferentially reflects or absorbs IR and transmits as much visible light as possible for the plants underneath. There exist several semi-transparent technologies focused on utilizing the IR solar spectrum, such as polymer solar cells with strong photosensitivity in the near-IR (NIR)(Chen, Dou, Zhu, Chung, Song, Zheng, Hawks, Li, Weiss & Yang, 2012), luminescent solar concentrators where a luminescent dye selectively absorbs UV and NIR and emits visible-wavelength light (Yang & Lunt, 2017), and thin planar NIR organic solar cells that can be used on architectural glass(Lunt & Bulovic, 2011). Nonetheless, such technologies are still in the development stage and do not have the efficiency and reliability of Si PV, a proven technology that had ~95% share of the worldwide PV production in 2017 (Philipps, 2019;Husain, Hasan, Shafie, Hamidon & Pandey, 2018). Figure 1b presents the solar spectral irradiance at ground level (the AM1.5) along with the absorption of a typical Si PV solar cell (ASTM, 2019). Si PV cells absorb photons with wavelengths below the Si bandgap (~1100 nm) (Smestad, 2002), including the 700-1100 nm region which accounts for ~34% of the total sunlight irradiance and visible light that accounts for another ~44%. Although the NIR band has less energy as compared to visible light, it has more photon numbers, 2391mol/sec/m², than that in the visible band (2121mol/sec/m²). Therefore, it is indeed economic to harvest NIR band for photovoltaics.

Here, we present a novel translucent solar module (TSM) which uses sparsely populated bifacial Si solar cells that absorb light through both the front and back sides, and cylindrical concentrating reflectors with a dichroic filter underneath (Fig. 2). A fraction of the incoming sunlight is absorbed directly by the front side of the solar cells. Light passing through the space between the solar cells encounters a concave shaped dichroic reflector. The reflector effectively acts as a spectrum-selective filter; NIR light between 700 and 1100 nm is reflected and concentrated to the backside of the solar cells, whereas the rest of the sunlight, including visible, UV light, and IR light > 1100 nm, is transmitted. The objective of this system is not to maximize concentration bur rather to optimize both the dichroic reflectance and the reflector shape to ensure adequate transmitted light and maximize PV conversion without the need to actively track the sun. This can help to have a reliable and cost-effective solution for BIPV greenhouse applications, where high visible light availability and high renewable energy generation are simultaneously satisfied.

2. Dichroic Design

The split spectrum design depends on several factors such as the plant-required spectrum, PV absorption spectrum, and concentration of the reflector. The dichroic reflector can be fabricated by depositing the designed coating on a flexible thin glass sheet such as Corning® *Willow*® glass (Showghi & Norwood, 2019), by adding a partially reflective polymeric thin film to slumped glass or highly transparent plastic surface, or by bending the film over a preassembled structure to achieve the desired curvature.

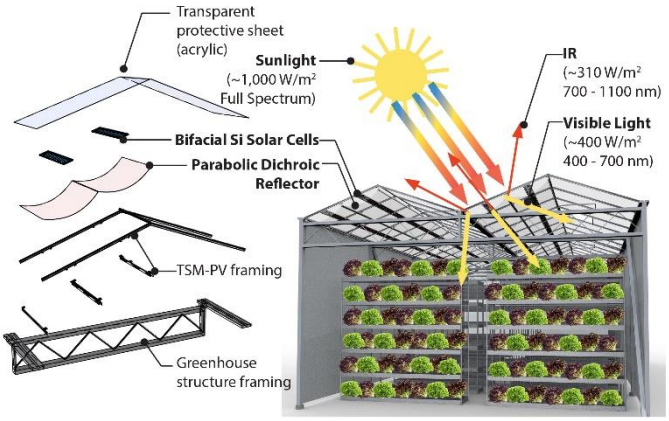

Figure 2. *Illustration of the translucent solar module (TSM) for greenhouse farming application.*

The dichroic reflectance per wavelength, $R(\lambda)$, was optimized by using the Si absorption, the PAR, and the available photon flux in the AM1.5 spectrum per wavelength, $N_{ph}(\lambda)$.The reflected solar irradiance, E_R, is a convolution of the $R(\lambda)$and the solar irradiance spectrum, E_s. While increasing the spectral range of $R(\lambda)$enhances PV production, it also reduces the illumination for the plants and thus it needs to be carefully selected. Moreover, the light illuminating the backside of the solar cell can be highly concentrated; hence it is necessary to also optimize the magnitude of $R(\lambda)$to avoid losses due to overheating. The overall average available irradiance for the solar cells (front and back sides) for a module with aperture collection width, D, and PV width, d (Fig. 3) is

$$E_{PV} = E_S + (S-1)\cdot E_R \tag{1}$$

where S is the fraction of non-PV populated area (the geometrical concentration for the backside of the solar cell). When the length of the PV and dichroic reflector are the same, this is defined as

$$S = D/d \tag{2}$$

The overall average available irradiance for the plants below the module is

$$E_{plants} = (1-1/S)\cdot(1-A)\cdot(E_S - E_R) \tag{3}$$

where A are losses due to absorption. Losses due to shadowing, sun motion, and secondary reflections can be calculated using ray tracing.

The design of the dichroic was optimized in Essential Macleod Thin Film software using $R(\lambda)$and a minimum number of layers to reduce cost. The dichroic was designed for incident angles at 45° to take into account blue shift effects (Miles, Cocilovo, Wheelwright, Pan, Tweet & Norwood, 2016) and the curvature of the reflector. The reflectance of an optimized dichroic coating with maximum $R(\lambda)$equal to 0.75, and spectral range from 750 to 1050 nm is shown in Fig. 4a. The coating requires only 14 layers of silicon dioxide (SiO_2) and aluminum oxide (Al_2O_3) on a glass substrate with refractive index, n, equal to 1.52.

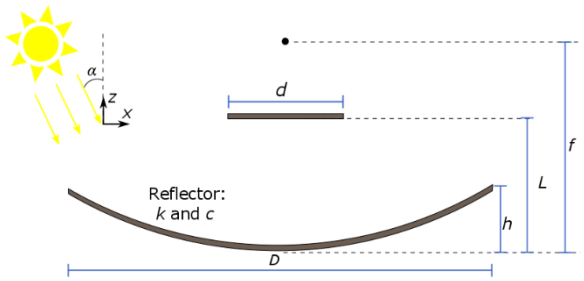

Figure 3.TSM using a conic section extruded reflector with conic constant, k, and, curvature, c. The FOV is calculated by changing the incident angle, α, of the sunlight about the y-axis.

There also exist readily available commercial thin film materials that have an acceptable reflectance spectrum for our application. In Fig. 4b, the reflectance spectrum of a self-adhesive polymeric window film is shown. The reflectance was measured with a spectrophotometer Agilent Cary 7000 using an N-BK7 substrate. Even though this film is not optimized, it presented an off-the-shelf solution for testing and fabricating a proof-of-concept TSM.

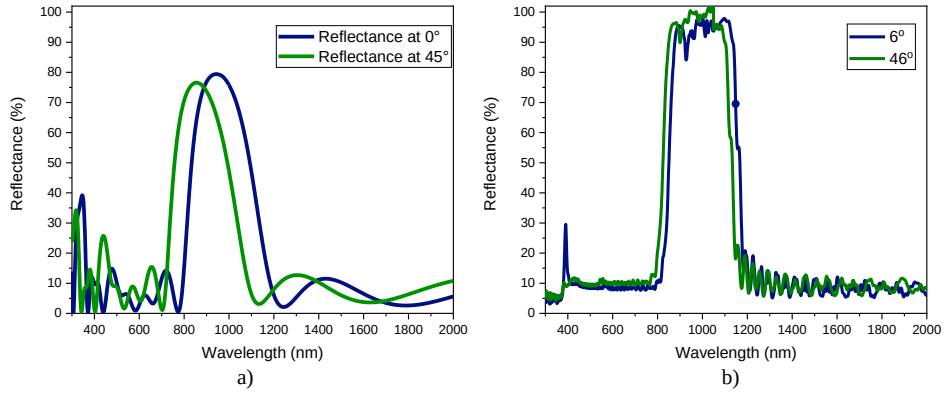

Figure 4. Dichroic filter for spectrum splitting: a) simulated reflectance spectrum of optimized dichroic filter at 45° incident angle for an S= ~5 TSM with reflectance peak around 75% and spectral range from 750 to 1050 nm; b)measured reflectance of commercial polymeric window films at two incident angles.

3. Reflector Optimization

The optimal shape of the dichroic reflector depends on the orientation and tilt of the installed translucent modules, desired concentration, physical area constraints, and the designed field-of-view (*FOV*) of the collector. The reflectors were designed as extruded conic section surfaces with conic constant, *k*, and, curvature, *c*:

$$y^2 = -2 \cdot V_r \cdot x + (k+1) \cdot x^2 \tag{4}$$

where V_r is the radius of curvature at the vertex equal to $1/c$ and the focal length (*f*) of the reflector is $V_r/2$ (Fig. 3).The *k* and *c* values were selected to maximize the total irradiance for all angles of the targeted *FOV* collected by the backside of the solar cell. The distance between the reflector vertex and the solar cell along the *z*-axis, *L*, was also optimized.

In order to quantify the collector *FOV*, the incident sunlight was tilted by an angle*a* about the *y*-axis. In the model, the *FOV* was defined as the largest incident angle for which the backside of the solar cell would collect at least 1/3 of the sunlight collected at normal incidence. For the present study, which includes field testing in Tucson, Arizona, the targeted *FOV* was around ±23.5° as this is the solar skew angle seasonal variability for an observer at 32.2° N latitude (Wheelwright, Angel, Coughenour, Geary & Stalcup, 2014).

The optimization of the reflector was done in the non-sequential ray tracing software Synopsys Light Tools (Fig. 5a-b). TheAM1.5 spectrum was included in the modeled solar source as well as non-sequential optical effects such as stray light and secondary reflections. During the optimization, the reflectors were treated as ideal perfect mirrors while the bifacial solar cell and frame parts were designed as ideal optical absorbers. The reflectivity, refractive index, and absorption values were taken from the Light Tools internal library.

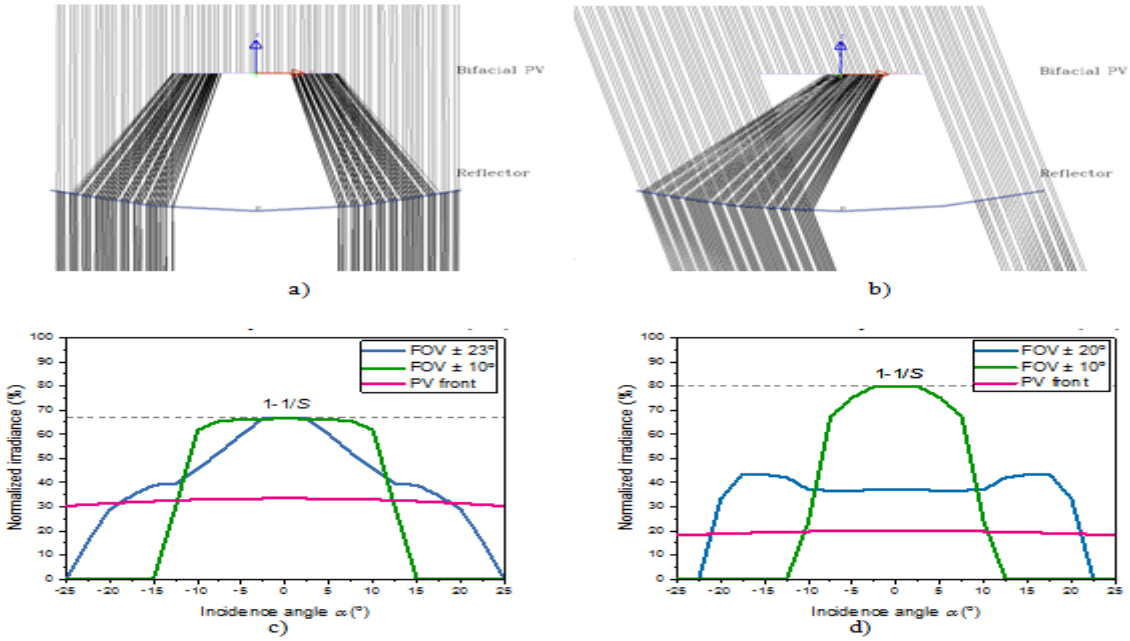

Figure 5. *Representative LightTools ray tracing simulations for an S = 2.2 TSM partially collecting sunlight at a) normal incidence (a = 0°) and at b) non-zero incidence angle (a = 15°). Optimization results for TSM with aperture d = 160 mm: c) S = 3 designed for FOV = ±23° (c = 0.0018 mm-1, k = 0, and L = -200 mm) and FOV = ±10° (c = 0.0016 mm-1, k = -1, and L = -300 mm) and a d) S = 5 TSM designed for FOV = ±20° (c = 0.00145 mm-1, k = -2, and L = -250 mm) and FOV = ±10° (c = 0.00115 mm-1, k = 0, and L = -400 mm). The PV front side collection is independent of the reflector shape.*

The results indicate that the geometry of the reflector strongly depends on *S*and the *FOV*. In Fig. 5(c-d), the irradiance collection of two *S* = 3and *S* = 5 reflectors, respectively, optimized to have *FOV*= ±23° and *FOV* = ±10°, is shown. The collectors achieve different collection profiles by varying *c*, *k*, and *L*. The normalized backside PV irradiance collection, η_C ,is defined as the fraction of incident light collected by the backside of the solar cell (ignoring losses due to absorption or partial reflectance). The maximum $\eta_C$is given by (1-1/*S*). The collection from the PV frontside is independent of the reflector shape and can achieve a 1/*S* maxima. In general, TSMs with small *S* require larger *c*'s than TSMs with relatively large *S* unless a non-zero *k* value is used. Moreover, systems with very large *S* (>5) tend to perform better if a small *FOV*(<±10°) is required. The ratio between V_r and *L* is usually between ~3.5-1.5in such a way that the *f*is above the PV cell, for systems with larger *FOV* (>±10°), or just below it, for systems with smaller *FOV*.

4. Fabrication and Testing

A full-size proof-of-concept TSM was fabricated as shown in Figure 6a. It consists of, from top to bottom, a 1.6-mm thick clear acrylic sheet as a top cover for three 156 x 156 mm² mono-crystalline bifacial Si solar cells connected in series and buried in Dow Sylgard™ 184 silicone, and a parabolic shaped reflector underneath. The reflector consists of a polymeric window film (described in the previous section) adhered onto a clear acrylic sheet that had been slumped into the designed parabolic curvature (*k* = -1 and *c* = to 0.0014mm^{-1} or V_r = 357 mm). A frame was added to keep the PV panel and the reflector at the designated position and separation as shown in Fig. 6b. The top cover and the dichroic reflector are similarly 410 mm wide. Taking the frame and the PV cell spacing into consideration, the proof-of-concept TSM has an *S*= ~2.2.

The current-voltage (*I-V*) characteristic curve was measured with a Keithley 2461 source meter while the TSM was mounted on a 2-axis tracker. Performance at different incidence angles was acquired by manually tilting the TSM East or West at various angles as referenced to the surface of the tracker while the tracker kept tracking the sun. Solar irradiance was measured with a Seaward Solar 200R irradiance meter mounted on the tracker. The irradiance on the front was measured to be between 1000 to 1050 W/m² whereas the irradiance reflected from the ground (albedo) was lower than 100 W/m², the detection limit of the unit; the air temperature was ~17°C.

The best metric for quantifying the efficacy of the TSM is the short-circuit current gain from the backside of the bifacial solar cells due to the presence of the dichroic reflector. Hence, a piece of aluminum (Al) foil, slightly larger than the string of solar cells, was placed on top of the acrylic sheet to block illumination from the front surface during the measurement (Fig. 6b).

The same set of measurements was repeated with and without the dichroic reflector. The difference between them is the $\Delta I_{SC,B}$ in which the contribution from the front surface and albedo is eliminated.

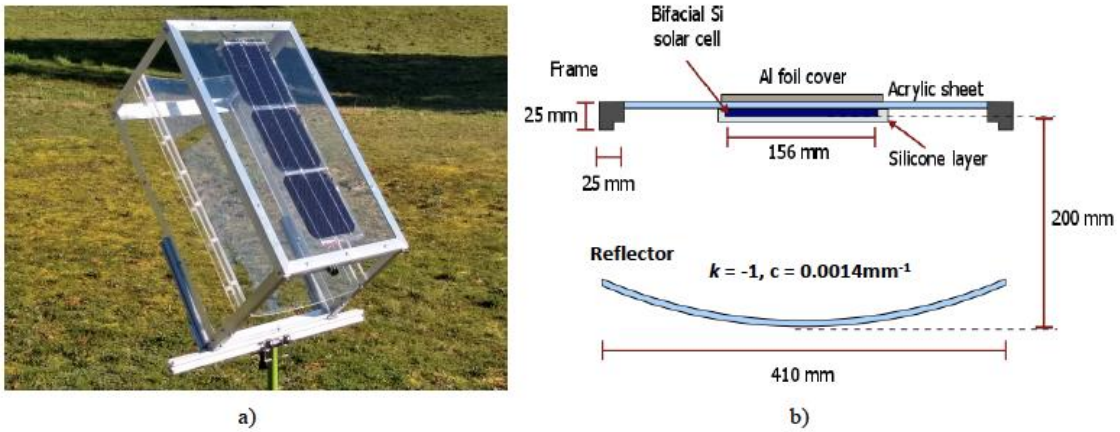

Figure 6. *TSM characterization: (a) proof-of-concept prototype on a stand facing the sun and b) cross-sectional schematic showing dimensions and components of the module.*

The performance enhancement can be expressed as $(\Delta I_{SC,B} + I_{SC,F})/I_{SC,F}$ where $I_{SC,F}$ is the nominal frontside short-circuit current of the solar cells, 9Amps in this case. This is the enhancement from a TSM over an otherwise identical mono-facial solar panel, and it can be readily derived from the $\Delta I_{SC,B}$ measurement procedure previously described.

To verify the measurement results, the $\Delta I_{SC,B}$ can be estimated from

$$\Delta I_{SC,B} = \eta_C \cdot S \cdot I_{SC,BT} \tag{5}$$

where η_C is obtained from ray tracing simulation and $I_{SC,BT}$ is the estimated short-circuit current from the backside of the solar cell that would be generated when illuminated under the portion of irradiance that the dichroic filter reflects,

$$I_{SC,BT} = q \cdot BF \cdot (1-OL) \cdot \int R(\lambda) \cdot EQE(\lambda) \cdot N_{PH}(\lambda) d\lambda \tag{6}$$

where q is the elementary charge, BF is the bifaciality factor of the solar cell (95.8%), OL represents the optical losses from the proof-of-concept TSM including8% from the front acrylic cover, 4% from the rear surface of the solar cell, and 7% from the shadowing by the metal busbars and grids on the solar cell, $R(\lambda)$ is the reflectance measured from the dichroic reflector (Fig. 4b), and EQE is the external quantum efficiency of a representative Si solar cell.

5. Results and Conclusions

In Fig. 7, the performance enhancement of the proof-of-concept TSM presents good agreement between the measurements and the calculations based on (5) and (6). Slight discrepancies between the measured and calculated results can be attributed to the fact that the reflectance of the dichroic reflector has angular dependence which is not considered in Eq. 6, the discrepancy between the representative EQE used in the calculation to the actual one, the finite unevenness and non-squareness of the frame, and the error from manually tilting the TSM at different angles. Nonetheless, the experimental results demonstrate that the proof-of-concept TSM with an S = ~2.2 generates, on average, ~25% more I_{SC} than a regular flat Si PV panel over a FOV of ±25°, while transmitting visible sunlight.

Our translucent solar module incorporates proven technologies to split visible and IR spectra and utilizes them in an efficient way. Experimental results from a 410 x 500 mm² proof-of-concept parabolic collector show excellent agreement with estimated values from PV principles, reflectance of a dichroic film, and ray tracing simulations, validating that we can optimize the TSM for different applications by changing the dichroic design and by varying the shape and dimensions of the reflector. Our technology improves the relative energy output of proven Si PV technology by capturing the reflected IR without substantial impact on the availability of visible light. This represents a cost-effective solution for operational energy and illumination use in greenhouse farming and building applications.

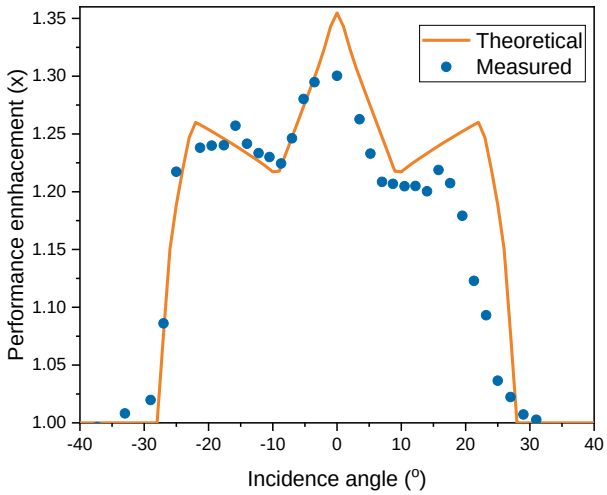

Figure7. Performance enhancement of the proof-of-concept TSM compared to estimated values. A collector of these dimensions can be used fora greenhouse pilot-scale application.

6. Notes about Architectural Integration

Based on the TSM design, physical prototype, and FOV optimization studies, the architectural integration of the modules with greenhouse construction is also designed for optimal structural and solar angle orientation.

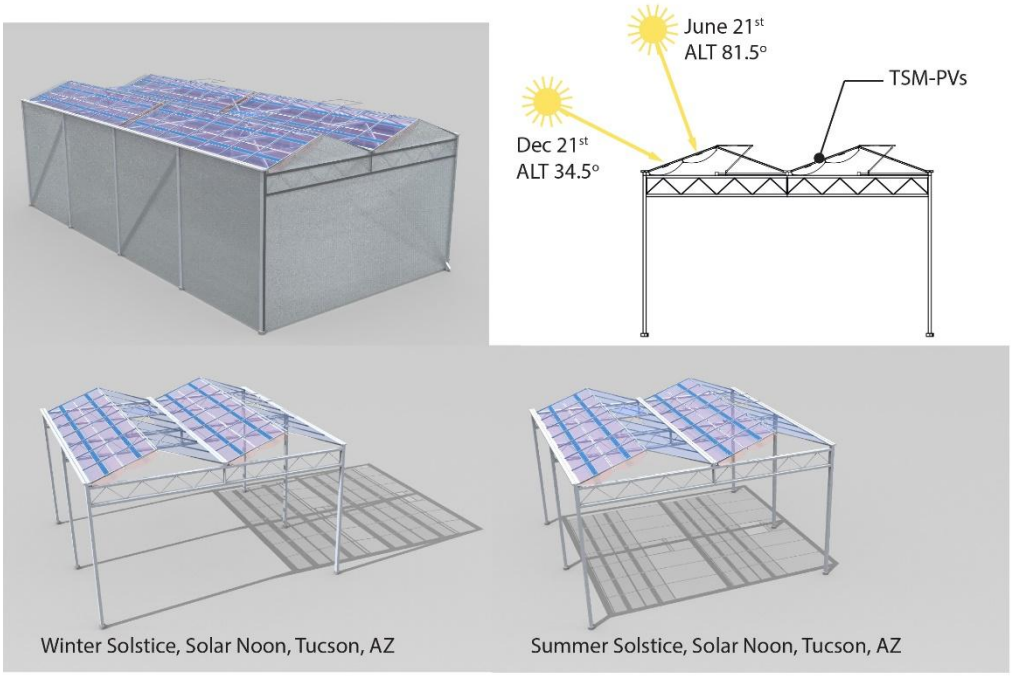

Figure8.TSM integration with greenhouse structure and local solar angle tilt optimization for PVs.

Standardized greenhouse structures are based on metal frame construction with lightweight truss members running horizontally and cross-bracing lateral members running diagonally around the outer perimeter. The lightweight metal frames are typically enclosed with a basic transparent plastic film for ease in deployment and optimal light transmission (Von Zabeltitz, 2011). The TSM-PV system is conceived to easily integrate into the standard greenhouse framing system for basic A-frame or sawtooth roof forms (Fig.8), which allow for the specific location sun angle tilt optimization. The prototype testing, which was conducted on a tracking apparatus, provided the ability to collect performance data at various incidence angles. The diagrams for TSM-PV greenhouse structure integration depict the optimal tilt-angle of the structure for solar noon sun angles in Tucson, AZ providing a range of absorption conditions from winter through summer solstice. Further analyses will be conducted for simulating the yearly performance output of the TSM-PV based on climate locations, integration of normalized prototype test-data, and structural tilt-angle orientations.

References

ASTM. (2019). Reference Solar Spectral Irradiance: Air Mass 1.5.*American Society for Testing and Materials, G-173*. Report retrieved from https://www.nrel.gov/grid-/solar-resource/spectra-am1.5.html

Barbosa, G., Kublik, N., Proctor, A., Reichelm, L., Weissinger, E., Wohlleb, G., & Halden, R. (2015). Comparison of Land, Water, and Energy Requirements of Lettuce Grown Using Hydroponic vs. Conventional Agricultural Methods. *International Journal of Environmental Research and Public Health, 12*(6), 6879.

Bisegna, F., Burattini,C.,& Mattoni,B. (2015). Lighting design for plant growth and human comfort.*Proceedings of 28th International Commission on Illumination, CIE 216*, Vol.1, Part 2.

Brown, P., & Wald, G. (1964). Visual Pigments in Single Rods and Cones of the Human Retina. *Science, 144*(3614), 45-52.

Chen, C., Dou, L., Zhu, R., Chung, C., Song, T., Zheng, Y., Hawks, S., Li, G., Weiss, P.S., & Yang, Y. (2012). Visibly transparent polymer solar cells produced by solution processing. *ACS Nano, 6*(8), 7185-7190.

Hassanien, R., Li, M., & Dong Lin, W. (2016). Advanced applications of solar energy in agricultural greenhouses. *Renewable and Sustainable Energy Reviews, 54*, 989-1001.

Heinstein, P., Ballif, C., & Perret-Aebi, L. (2013). Building Integrated Photovoltaics (BIPV): Review Potentials Barriers and Myths. *Green, 3*(2), 125-156.

Husain, A., Hasan, W., Shafie, S., Hamidon, M., & Pandey, S. (2018). A review of transparent solar photovoltaic technologies. *Renewable and Sustainable Energy Reviews, 94*, 779-791.

Lunt, R., & Bulovic, V. (2011). Transparent, near-infrared organic photovoltaic solar cells for window and energy-scavenging applications. *Applied Physics Letters, 98*(11).

Miles, A., Cocilovo, B., Wheelwright, B., Pan, W., Tweet, D., & Norwood, R. (2016). Designing spectrum-splitting dichroic filters to optimize current-matched photovoltaics. *Applied Optics, 55*(8), 1849-1853.

Parida, B., Iniyan, S., & Goic,R.(2011). A review of solar photovoltaic technologies.*Renewable and Sustainable Energy Reviews,15*(3), 1625-1636.

Philipps,S. (2019). Photovoltaics report. *Fraunhofer Institute for Solar Energy Systems ISE*, *March.*Report retrieved from https://www.ise.fraunhofer.de/en-/publications/studies/photovoltaics-report.html

Showghi, S.A.,&Norwood, R.A. (2019). *Flexible curved components for providing spectral characteristics for large surfaces.* PCT/US2019/020013.

Smestad, G. (2002). *Optoelectronics of solar cells (SPIE monograph ; 115).*Bellingham, WA: Society of Photo-optical Instrumentation Engineers.

Sun, J., Nishio, J., & Vogelmann, T. (1998). Green Light Drives CO 2 Fixation Deep within Leaves 1. *Plant and Cell Physiology, 39*(10), 1020-1026.

Tibbits, T. W. (1993). Terminology of photosynthetically active radiation for plants.*CIE Collection in Photobiology and Photochemistry*, *CIE 106* (8).

US EIA. (2016). 2012 Commercial Buildings Energy Consumption Survey. *U.S. Energy Information Administration,CBECS*. Report retrieved from https://www.eia.gov-/energyexplained/index.php?page=us_energy_commercial

Von Zabeltitz, C. (2011). *Greenhouse Structures*. In Integrated Greenhouse Systems for Mild Climates: Climate Conditions, Design, Construction, Maintenance, Climate Control (First ed., pp. 59-135). Berlin, Heidelberg: Springer Berlin Heidelberg.

Wheelwright, B., Angel, Coughenour, Hammer, Geary, & Stalcup. (2014). Field weighting model for tracking-integrated optics. *AIP Conference Proceedings, 1616*(1), 237-241.

Yang, C., & Lunt,R.R.(2017). Limits of visibly transparent luminescent solar concentrators.*Advanced Optical Materials. 5,* 1600851.